

УДК 534.8+551.55

**CHARACTERIZING AND MODELLING OCEAN AMBIENT NOISE  
USING INFRASOUND NETWORK AND MIDDLE ATMOSPHERIC MODELS**<sup>1,2)</sup> M. De Carlo, <sup>1)</sup> A. Le Pichon, <sup>3)</sup> F. Ardhuin, <sup>4)</sup> S.P. Näsholm<sup>1)</sup> *The Atomic Energy Commission (CEA/DAM/DIF), Arpajon, France*<sup>2)</sup> *University of Western Brittany (UBO), Brest, France*<sup>3)</sup> *French Research Institute for the Exploitation of the Sea (IFREMER, LPO/CNRS), France*<sup>4)</sup> *NORSAR, Kjeller, Norway*

Infrasound is one of the technologies of the International Monitoring System (IMS) supporting the verification regime of the Comprehensive Nuclear-Test-Ban Treaty (CTBT). In the frequency band of interest to detect atmospheric explosions, ambient noise may affect detection and particularly ocean noise referred to as microbaroms. Ocean wave interactions generate acoustic noise almost continuously which can obscure signals of interest in their frequency range. The detectability of such noise strongly depends on atmospheric conditions along the propagation paths. Using ocean wave action model developed by IFREMER and considering the effects of general middle-atmospheric products delivered by ECMWF in long-range propagation, microbarom amplitudes and direction of arrivals derived from various propagation models are compared with the observations. With this study, it is expected to enhance the characterization of the ocean-atmosphere coupling. In return, a better knowledge of microbarom sources would allow to better characterize explosive atmospheric events hidden in the ambient noise.

**INTRODUCTION**

Within the framework of the Comprehensive Test Ban Treaty (CTBT), the infrasound stations of the International Monitoring System (IMS) detect a continuous noise of ocean origin between 0.1 and 0.5 Hz. The amplitude of this noise, referred to as microbaroms, can be quite important and hide signals of interest for the CTBTO monitoring purpose [1]. It has been shown that microbaroms are generated by the ocean and particularly by severe storms over the ocean [2]; [3]. Due to this localization and their frequency they were early compared with microseisms – noise in seismic signals, assuming a common source phenomenon for both microbaroms and microseisms [3, 4]. Longuet-Higgins first developed in 1950 a theory about microseisms generation. Whereas first order interactions between ocean and atmosphere only generate evanescent pressure terms, second order interactions generate propagating pressure waves, that transfer energy through the ocean bottom and propagate into the crust [5]. Hasselmann extended this second order interaction theory for broad band spectrum [6] and generalized it in the framework of wave-wave interactions [7]. Applying the revisited Longuet-Higgins-Hasselmann's theory to wave-action models, a microseism source model has been developed [8] and distributed by IFREMER. This source model has been used and validated with microseismic observations [9, 10].

The generation of microbaroms was investigated theoretically on the basis of the microseisms theory [11–13]. Although these theories have in common the Hasselmann's integral:  $\int E(f, \theta)E(f, \theta + \pi)d\theta$ , which corresponds to the coupling terms between two opposing waves, where  $E(f, \theta)$  is the wave height spectrum over the direction  $\theta$ , they differ quantitatively. Furthermore, to explain microbarom observations, the effects of long-range propagation through a realistic atmosphere should

be modeled as these effects can be sources of uncertainties. Thus, studies that have been carried out comparing models and observations remain mainly qualitative [14].

To propagate infrasound signals, a suite of full wave propagation models - such as ray-tracing, parabolic equation, modal mode expansion methods - was developed by many researchers [15]. They require relatively low computing time when assuming range independent atmosphere along the propagation path. Full-wave equation model was not considered in this study for computational reasons. The propagation of infrasound is strongly affected by the velocity structure of the middle-atmosphere; leading to the necessity of using realistic atmospheric specifications. The European Centre for Medium-Range Weather Forecasts (ECMWF) develops atmospheric models. Although these models have been improving significantly in recent years with data assimilation and reanalysis, they are known to be inaccurate above ~40 km altitude where very few in-situ measurements can be realized [16]. Unfortunately, the middle atmosphere (30–90 km altitude) is of importance for infrasound propagation due to the fact that acoustic ducts can occur at these altitudes. Studies have shown how infrasound detection from identified and calibrated natural sources can provide additional useful constraints of unresolved atmospheric structures in range of altitude where routine observations are lacking [17]. Microbaroms being a continuous source of infrasound, it is expected that their global monitoring could contribute to an improved description of dynamical properties of the atmosphere. It is thus essential to determine a reliable source and propagation model, to estimate errors. In this study, the methodological aspect is addressed, using a simplified approach, and considering separately the impact of both source and propagation models to predict microbarom observations.

## METHODS AND DATA

### Studied area and dates

Two years of infrasound recordings at the Norwegian IMS station IS37 are investigated. This station, located 69.075°N and 18.6°E continuously receive signals originating both from the Atlantic Ocean and the Sea of Barents. Amplitude of these sources of microbaroms is much higher in winter than in summer and these seasonal variations are presented in Figure 1 along with the location of the station. IS37 consists of 10 microbarometers, with an aperture of 2 km. The time-signals are processed with processing multi-channel correlation (PMCC) algorithm [18] which uses correlation time delays between sensors and sub-networks to estimate wavefront parameters, such as back-azimuth, root-mean-square amplitude and frequency, of coherent planar waves. To do so, the algorithm searches for coherent signals in advancing time windows over a set of 15 log-spaced frequency bands between 0.01 and 5 Hz. Frequency bands are defined here with Chebyshev filters of order 2 and the use of log-spaced frequency bands enhance signal discrimination [19].

### Data sources

For the simulation, we use the WaveWatch3 (WW3) wave action model developed by NOAA (National Oceanic and Atmospheric Administration) and distributed by IFREMER (<ftp://ftp.ifremer.fr/ifremer/ww3>), with a spatial-resolution of 0.5° and a temporal resolution of 3 h. Ardhuin et al, 2011 [8] implemented the microseism source as a composite from WW3 results, according to the formula:

$$P2L = \frac{\pi \omega_s^2}{\alpha_w^2} \rho_w^2 g f_s E^2(f) I(f)$$

where  $f_s = \frac{\omega_s}{2\pi} = 2f$  is the frequency of microbaroms (Hz),  $f$  being the sea state frequency (Hz),  $\alpha_w$  is the

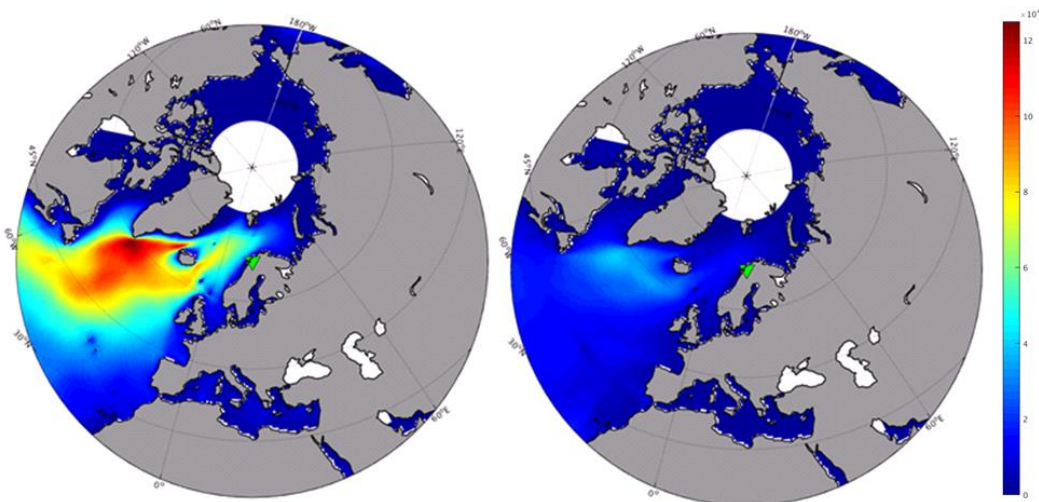
sound speed in water ( $m \cdot s^{-1}$ ),  $\rho_w$  is the water density ( $kg \cdot m^{-3}$ ),  $g$  the gravitational acceleration ( $m \cdot s^{-2}$ ) and  $E^2(f)I(f)$  is the wave interaction term such as  $E^2(f)I(f) = \int E(f, \theta)E(f, \theta + \pi)d\theta$ . Source term P2L is in  $Pa^2 m^2 s^{-1}$ .

It is known that the amplitude of microbarom source is different from the one of microseism source. However, microbarom source is supposed to be proportional to microseism, thus for a qualitative work, microseism source can be used as it is already calculated. This source is named ‘P2L’ in IFREMER database, and corresponds to the acoustic spectral density.

To account for propagation, the infrasound propagation losses formula presented in [19] is used. The formula was based on numerous Parabolic Equations simulations of infrasound through simple range-independent atmosphere models, varying frequency and ratios of effective sound speed. The attenuation coefficient (dimensionless) from a point situated 1 km from the source is given by:

$$Att = \frac{10^{\frac{\alpha(f)R}{20}}}{R} + \frac{R^{\beta(f, V_{eff-ratio})}}{1 + 10^{(\delta-R)/\sigma(f)}}$$

where  $\alpha$  (in  $km^{-1}$ ),  $\beta$ ,  $\delta$  (in  $km$ ),  $\sigma$  (in  $km$ ) are parameters tabulated in [19],  $V_{eff-ratio}$  is the dimensionless ratio of the effective sound speed within stratosphere to that at ground level,  $f$  is the signal frequency (in Hz) and  $R$  is the distance from the source (in  $km$ ). So the pressure amplitude is:  $A(f, R, V_{eff-ratio}) = A_{1km} * Att$ . As this formula was developed for a range-independent atmosphere, a strong assumption is made by choosing a uniform  $V_{eff-ratio}$ . The wind at the station location being the most relevant choice to characterize whether the station will receive a signal, it is then the value used for  $V_{eff-ratio}$ .



Green triangle is the location of the IS37 station

Figure 1. Source of microbaroms in  $Pa^2 m^2 s^{-1}$  (WW3) averaged over January (left) and July (right)

Atmospheric data at the station have been obtained from the operational ECMWF high-resolution (HRES) atmospheric model with temporal resolution of 6 hours. The wind is averaged between 40 and 60 km of altitude in order to integrate altitudes of interest.

### Simulation

In order to sample correctly the grid for the simulations, 360 paths are drawn from the station –with constant azimuth direction along the path – creating an azimuthal grid of  $1^\circ$  resolution. For each path, intersected source cells are selected, and the attenuation given both by the distance between the cell and the station and by the wind projected along the azimuth is computed. After applying the attenuation to the source, all attenuated sources are summed along the path to obtain the directional pressure density spectrum.

In this study, three simulations are carried out : (i) the first one focuses on wind effect assuming a constant source all over the ocean ( $p2l = 1$ ), (ii) the second one includes p2l model, but does not consider wind effect ( $V_{eff-ratio} = 1$ ) to address source effect, and (iii) the last one combines wind and source effects.

As a result of simulation  $A(f, \theta)$  is obtained for each time step (*i.e.* every 6 hours) where  $A$  is the amplitude (in  $Pa$ ) and  $\theta$  is the azimuth. For comparisons with the observations, it is assumed that signals with the largest amplitude are most likely to be detected. So for each time step:  $A_{mod}(\Delta t) = \max_{(f, \theta)} A(f, \theta)$  and  $\theta(t) = \theta_m$  with  $\theta_m$  is such as  $A(f_m, \theta_m) = \max_{(f, \theta)} A(f, \theta)$ . The same process is applied to observations whenever there is more than one detection in the time step:  $A_{obs}(\Delta t) = \max_{t \in \Delta t} A(t)$  and the azimuth is the azimuth corresponding to this particular amplitude.

### RESULTS

From January 2016 to the end of March 2018, 76 035 detections are obtained at IS37, with time gaps between two detections quite heterogeneous varying from 2.3 s to some days, when the signals are too noisy. Figure 2 shows the number of detections per modelling time step, which varies greatly between few detections to some tens of detections per 6 hours.

### Wind effect

In Figure 3, the results of the first simulation – wind effect only – are presented in blue and the observations in orange. The upper graph corresponds to the azimuth as seen at the station and the lower one corresponds to the amplitude. A higher dispersion in the observed azimuth is noticed in summer – from  $-90^\circ$  to  $90^\circ$  – compared to winter – around  $90^\circ$ , which coincides with lower amplitude of the observed signal, whereas in summer the model predicts a very precise azimuth around  $45^\circ$ . However, this precision is only an artefact of the simulation due to the large range of azimuths – from  $20^\circ$  to  $45^\circ$  (not shown here) – with the same amplitude in summer. During winter, azimuthal comparison between simulations and observations yields better results. For the amplitude, seasonal variations result from both wind effect and source size effects. Indeed as the contributions are summed and the source is set to constant all over the ocean, the longer the ocean in one direction, the higher the cumulated amplitude. This simulation points out the impact of wind variations: in winter eastward winds allow IS37 to detect source in North Atlantic ( $-90^\circ$ ) whereas in summer, westward winds hide the North Atlantic source allowing IS37 to detect source from the Barents Sea (between  $0$  and  $45^\circ$ ).

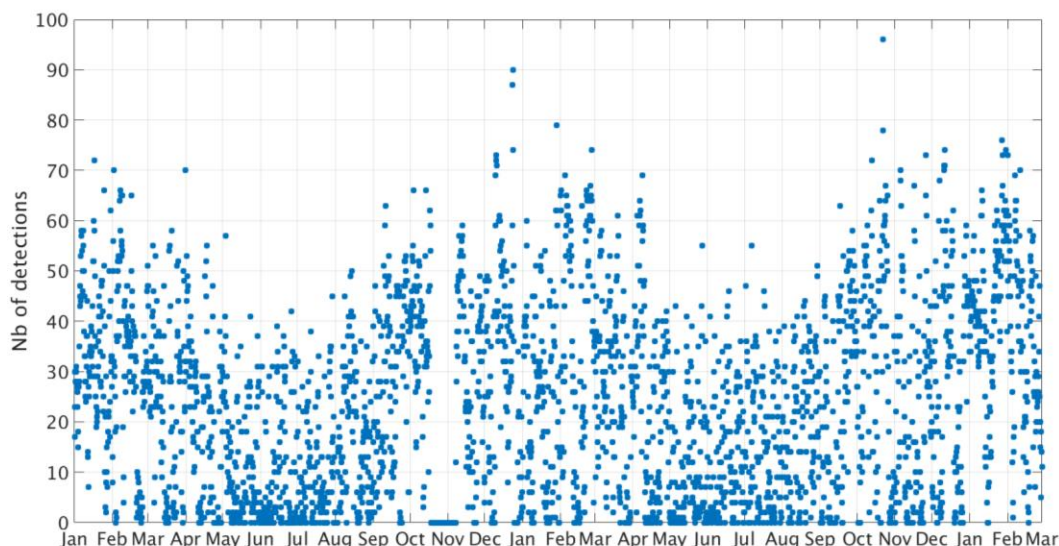


Figure 2. Number of detections per time step (6 hours)

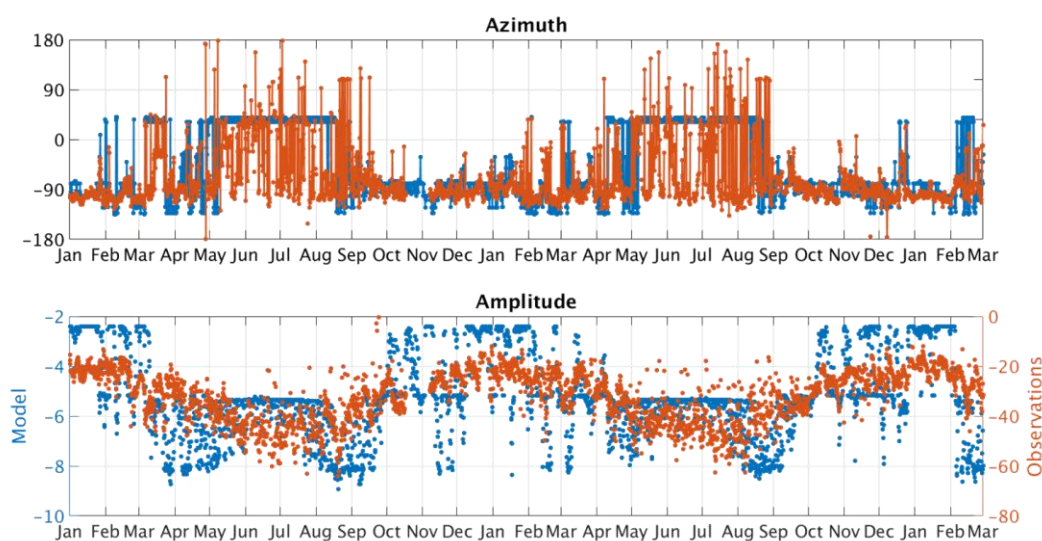


Figure 3. Comparisons between modeled (blue) and observed (orange) azimuth and amplitude. Source term is set uniformly to 1

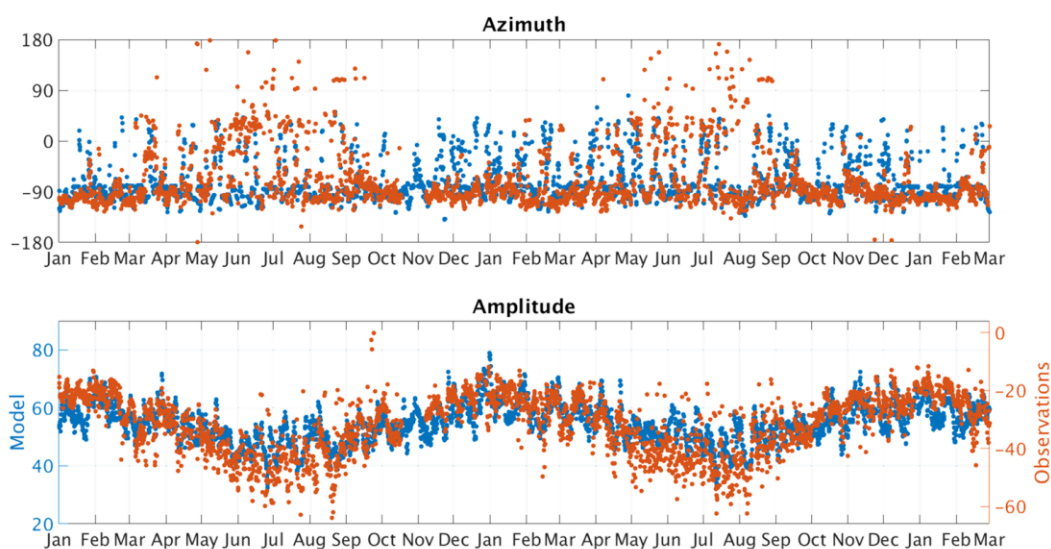


Figure 4. Comparisons between modeled (blue) and observed (orange) azimuth and amplitude. Effective wind ratio is set to 1

#### Source effect

Second simulation – about source effect, without wind – is presented in Figure 4. Concerning the azimuth, a preferential direction around  $-90^\circ$  – corresponding to the Atlantic Ocean – may be seen both for simulations and observations, with some azimuthal dispersion up to  $45^\circ$ . Difference between observations and simulation results occurs mostly in winter, when the azimuthal dispersion is much smaller in the observations: azimuth varies around  $-90^\circ$  in the observations, whereas it varies from  $-110^\circ$  to  $45^\circ$  for the simulation results. Concerning the amplitude, although there is a systematical offset of around 80 dB between both cases, there are seasonal variations with lower amplitudes in summer and higher ones in winter. It can be noted that

the amplitude of the seasonal variations is of 30 dB for the observations whereas only about 15 dB for the simulation.

#### Complete simulation: wind and source effect

Figure 5 presents the same results for the third simulation including both atmospheric and source effects. It shows a really good agreement between simulation results and observations: dominant azimuth is  $-90^\circ$ , with high azimuthal dispersion (from  $-90^\circ$  to  $45^\circ$ ) from May to September, and quite a narrow dispersion from October to April. Simulations reproduce well the amplitude seasonal variations – for both observation and simulation the amplitude of seasonal variations is  $\sim 30$  dB – along with some second order amplitude variations.

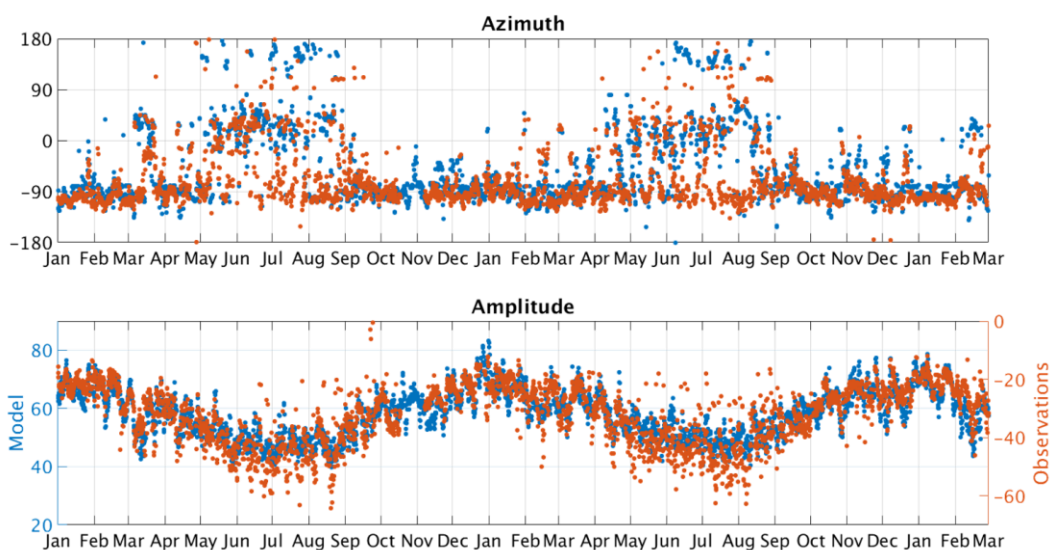


Figure 5. Comparisons between modeled (blue) and observed (orange) azimuth and amplitude. Both atmospheric model and source model are used

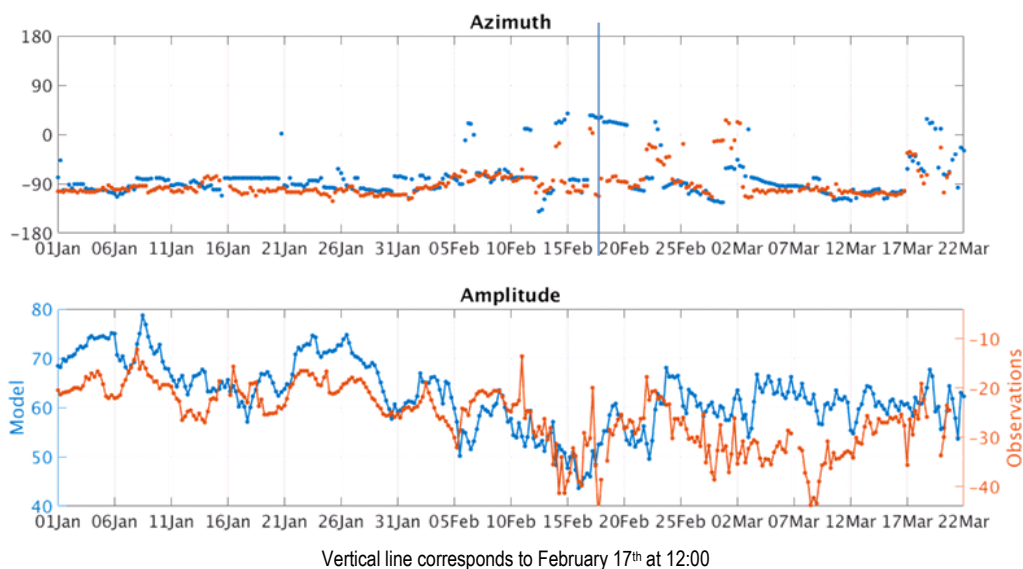


Figure 1. Zoom - Comparison for azimuth and amplitude between observations (orange) and simulation 3 (blue). Both atmospheric model and source model are used

Some conclusions can be drawn from the comparison of the three simulations:

- During summer, the source is clearly the dominant factor of the detected signal, as there is no significant change between simulation (ii) and (iii), wind only enhances the attenuation of the signal.
- In the contrary, during winter sources are more spatially scattered, and wind becomes more important by discriminating the sources.
- The higher dispersion of sources in winter might be due to an increase of the number of storms during this season; storms being one of the main factor generating opposing waves [8].

At first order, simulation with modeled source and uniform wind equal to the wind at the station fits well

with the observations. Some second order features can also be seen as similar: Figure 6 focuses on the period between January 2018 and March 2018. In January there is a different offset between observed and simulated amplitude – 90 dB – but trends are similar. Then, good agreement in azimuth and amplitude trends can be seen. However, for some specific days – between February 10<sup>th</sup> and 20<sup>th</sup> – the simulation presents a higher azimuth deviation – simulated azimuth is around 20 to 45° whereas observed one is between –20° and 20°. In addition, this azimuth deviation lasts longer than the one of the observations – from two to four days, while observed azimuth deviation is around 12 hours. Around March 10<sup>th</sup>, a discrepancy in amplitude is also noted.

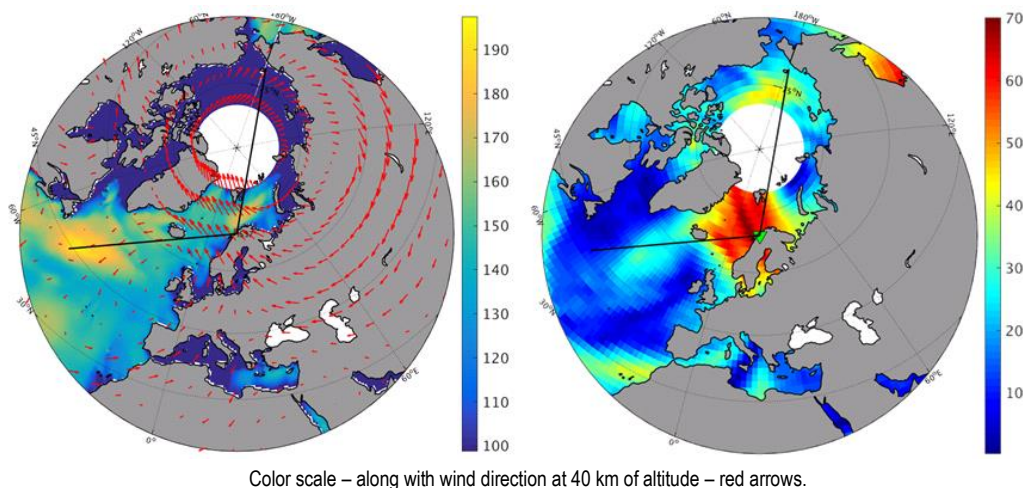


Figure 7. Wind conditions for February 17<sup>th</sup> 2018 at 12:00, with path at 10° and -90° azimuth – black lines.  
Left panel: Microbarom source term (in dB) Right panel: intensity of winds in  $m.s^{-1}$

An explanation to these differences could be additional atmosphere effects along the path which are not here considered. The atmosphere characteristics during this period, presented on Figure 7, seem to support this suggestion. Indeed, wind at the station is directed towards North-West, and it is less favorable to the North Atlantic source compare to the Barents Sea source. However, considering the path from source to station, there are strong opposing winds from the Barents Sea source, whereas from North Atlantic source, opposing winds are rather weak.

#### DISCUSSION AND CONCLUSIONS

The atmospheric and source effects on microbaroms detection were investigated by comparing simulations with observations at IMS Norwegian station IS37. It was found that the source effect is the most important one to explain the main observed features of the azimuth (dominant azimuth) and amplitude (seasonal variations). However, it was shown that atmospheric effects should also be considered, particularly in winter, when winds are stronger and sources are more numerous and scattered. Indeed, wind allows discriminating between sources, and modulating the amplitude, yielding to comparable seasonal variations of ~30 dB between winter and summer.

Results at first order correlate well the observations, which is quite encouraging due to the simplicity of the atmospheric model used. Some second order features are also coherent with the observations which support the choice of atmospheric specifications given at the station. However, some discrepancies appear during particular atmospheric events – mid-February 2018 – such as Sudden Stratospheric Warming (SSW). A SSW consists in a warming of the stratosphere, modifying atmospheric characteristics such as winds and they have a cooling impact on the lower layers of the atmosphere, generating what we know as cold wave. Usually during winter, wind vortex is well established towards the East, however, during these phenomena, the vortex is dis-

turbed and can be broken, modifying the duct for infrasound propagation [20]. These discrepancies may be explained by additional atmospheric effects that were not accounted for.

IS37 is an interesting station due to its location close to the Barents Sea where sources generated are weaker than in the Atlantic Ocean. Then, unlike other IMS stations, IS37 has the capability of detecting signal from both sources, in the same frequency-band. When the two sources are in competition, this could be problematic for PMCC processing as it is designed to detect the most coherent signals in a given time and frequency window. Hence, signal processing issues are another possible explanation of the discrepancies seen during 2018 SSW.

The propagation was simulated by a simple range-independent attenuation relation that accounted for the capability of the station to receive the signal. Further studies should be pursued to integrate range-dependent atmospheric characteristics to take into account variations along the path that could strengthen or weaken the attenuation of the source, leading to a possible change of the dominant received signal. Other propagation models, accounting for azimuth deviation, could also be investigated to enhance second order fitting of simulations and observations.

Methodology should also be addressed in future work by exploring other processing methods (e.g. FK analysis, MUSIC) in addition to PMCC, in order to validate the comparisons between simulations and observations data. Indeed, having comparable data and formats of data could allow us to define a metric of error and correlation between observations and simulations. Moreover, quantifying the source is another methodology issue to be addressed, so to do quantitative comparisons: acoustic impedance might be added to P2L term, at least. Bathymetric effects in regards to directionality of the acoustic waves should also be investigated for source quantification.

## REFERENCES

1. Campus, P. Worldwide observation in infrasonic waves / P. Campus and D. Christie // *Monitoring for Atmospheric studies*, Springer Geosciences, ISBN: 978-1-4020-9507-8, 2010. – P. 185–234.
2. Donn, W. Infrasonic waves from the marine storm of April 7, 1966 / W. Donn and E. Posmentier // *J. Geophys. Res.* – 1967. – no. 72. – pp. 2053–2061.
3. Donn, W. Sea wave origin of microbaroms and microseisms / W. Donn and B. Naini // *J. Geophys. Res.*, 1973. – no. 78. – P. 4482–4488.
4. Rind, D. Microseisms at Palisades 3. Microseisms and microbaroms / D. Rind // *J. Geophys. Res.*, 1980. – no. 85. – P. 4854–4862.
5. Longuet-Higgins, M. A theory of the origin of microseisms / M. Longuet-Higgins // *Phil. Trans. R. Soc. Lond.*, 1950. – vol. A, no. 243. – P. 1–35.
6. Hasselmann, K. A statistical analysis of the generation of microseisms / K. Hasselmann // *Rev. Geophys.*, 1963. – vol. 2, no. 1. – P. 177–210.
7. Hasselmann, K. Feynman diagrams and interaction rules of wave-wave scattering processes / K. Hasselmann // *Rev. Geophys.*, 1966. – vol. 1, no. 4. – P. 1–32.
8. Arduin, F. Ocean wave sources of seismic noise / F. Arduin, E. Stutzmann, M. Schimmel and A. Mangeney // *J. Geophys. Res.*, 2011. – no. 116.
9. Gualtieri, L. Modelling secondary microseismic noise by normal mode summation / L. Gualtieri, E. Stutzmann, Y. Capdeville, F. Arduin, M. Schimmel, A. Mangeney and A. Morelli // *Geophys. J. Int.*, 2013. – no. 193. – P. 1732–1745.
10. Sergeant, A. Frequency-dependent noise sources in the North Atlantic Ocean / A. Sergeant, E. Stutzmann, A. Maggi, M. Schimmel, F. Arduin and M. Obrebski // *Geochem. Geophys. Geosyst.*, 2013. – vol. 14, no. 00.
11. Brekhovskikh, L. Radiation of infrasound into atmosphere by surface-waves in ocean / L. Brekhovskikh, V. Goncharov, V. Hurtepov and K. Naugolny // *Izvestiya Akademii Nauk SSSR Fizika Atmosfery i Okeana*, 1973. – vol. 9, no. 9. – P. 899–907.
12. Waxler, R. The radiation of atmospheric microbaroms by ocean waves / R. Waxler and K. Gilbert // *J. Acoust. Soc. Am.*, 2006. – vol. 119, no. 5. – P. 2651–2664.
13. Arduin, F. Noise generation in the solid Earth, oceans and atmosphere, from nonlinear interacting surface gravity waves in finite depth / F. Arduin and T. H. C. Herbers // *J. Fluid Mech.*, 2013. – vol. 716. – P. 316–348.
14. Assink, J. Bidirectional infrasonic ducts associated with sudden stratospheric warming events / J. Assink, R. Waxler, P. Smets and L. Evers // *J. Geophys. Res. Atmos.*, 2014. – vol. 119. – P. 1140–1153.
15. Waxler, R. Propagation modelling through realistic atmosphere and benchmarking / R. Waxler and J. Assink // *Infrasound Monitoring for Atmospheric Studies: Challenges in Middle-atmosphere Dynamics and Societal Benefits*, Springer Nature, 2018.
16. Le Pichon, A. Comparison of co-located independent ground-based middle-atmospheric wind and temperature measurements with Numerical Weather Prediction models / A. Le Pichon, J. Assink, P. Heinrich, E. Blanc, A. Charlton-Perez, C. Lee, P. Keckhut, A. Hauchecorne, R. Rüfenacht and N. Kämpfer // *J. Geophys. Res. Atmos.*, 2015. – vol. 120.
17. Assink, J. Evaluation of wind and temperature profiles from ECMWF analysis on two hemispheres using volcanic infrasound / J. Assink, A. Le Pichon, E. Blanc, M. Kallel and L. Khemiri // *J. Geophys. Res. Atmos.*, 2014. – vol. 119.
18. Y. Cansi, An automatic seismic event processing for detection and location: The PMCC method / Y. Cansi // *Geophys. Res. Letters*, 1995. – vol. 22, no. 9. – P. 1021–1024.
19. Le Pichon, A. Recent enhancements of the PMCC infrasound signal detector / A. Le Pichon, R. Matoza, N. Brachet et Y. Cansi // *Inframatrics*, 2010. – vol. 26. – P. 5–8.
20. Le Pichon, A. Incorporating numerical modeling into estimates of the detection capability of the IMS infrasound network / A. Le Pichon, L. Ceranna and J. Vergoz // *J. Geophys. Res. Atmos.*, 2012. – vol. 117, no. D5.
21. Smets, P. The life cycle of a sudden stratospheric warming from infrasonic ambient noise observations // *J. Geophys. Res. Atmos.*, 2014. – vol. 119, no. 21. – P. 12084 – 12099.

## ИНФРАДЫБЫСТЫҚ ЖЕЛІСІ МЕН ЖЕЛ МОДЕЛЬДЕРІН ПАЙДАЛАНЫП МҰХИТТИҢ ШУ АЯСЫНЫҢ СИПАТТАМАСЫ МЕН МОДЕЛЬДЕУІ

<sup>1,2)</sup> Де Карло М., <sup>1)</sup> Ле Пишон А., <sup>3)</sup> Ардуин А., <sup>4)</sup> Нэшолм С.П.

<sup>1)</sup> *Атом энергиясы жөніндегі комиссариаты (CEA/DAM/DIF), Арпажон, Франция*

<sup>2)</sup> *Батыс Бретан Университеті (UBO), Брест, Франция*

<sup>3)</sup> *Франция Теңіз пайдалану ғылым-зерттеу институты (IFREMER, LPO/CNRS), Франция*

<sup>4)</sup> *NORSAR, Кьеллер, Норвегия*

Халықаралық мониторинг жүйесі (ХМЖ) атмосфералық жарылыстар мен тәрізді оқиғаларды айқындауына пайдаланылады. Зерттелудегі жиіліктер жолағында шу аясы табылған оқиғасына әсерін тигізу мүмкін, ерекшелігінде, микробаромдар ретінді белгілі болатын мұхиттің шулы аясы. Мұхиттағы толқындардың өзара әрекеттестігі акустикалық шуды тұрақты өндіріп тұрады, бұл қызықтыратын сигналдарды жасыру мүмкін. Сондай шудың ықпалы ол таралу трассасы бойындағы атмосфералық жағдайларына байланысты. IFREMER океанографиялық институтымен (Франция) әзірленген мұхит толқындарының өзара әрекеттестігі моделін және, ECMWF (Ауаны ортамерзімдік болжау еуропалық орталығы) беріп тұратын, жаһандық атмосфералық

модельдердің әсерлерін есепке ала отырып, авторлар бақылаудың әр түрлі модельдерінде микробаромдардың амплитудалары мен азимуттарын салыстырады. Бұл зерттеу атмосфера мен мұхиттің өзара әрекеттестігінің сипаттамаларын жақсартады деп күтілуде. Өз кезегінде, микробаромдар көздері туралы білімдерді арттыруы атмосфералық жарылыс оқиғаларды одан жақсы сипаттауына мүмкіншілік береді.

### ОПИСАНИЕ И МОДЕЛИРОВАНИЕ ШУМОВОГО ФОНА ОКЕАНА С ПОМОЩЬЮ ИНФРАЗВУКОВОЙ СЕТИ И МОДЕЛЕЙ ВЕТРА

<sup>1,2)</sup> Де Карло М., <sup>1)</sup> Ле Пишон А., <sup>3)</sup> Ардуин А., <sup>4)</sup> Нэшоулм С.П.

<sup>1)</sup> *Комиссариат по атомной энергии (CEA/DAM/DIF), Арнажон, Франция*

<sup>2)</sup> *Университет Западной Бретани (UBO), Брест, Франция*

<sup>3)</sup> *Французский научно-исследовательский институт по эксплуатации моря (IFREMER, LPO/CNRS), Франция*

<sup>4)</sup> *NORSAR, Кьеллер, Норвегия*

Инфразвуковая сеть Международной системы мониторинга (МСМ) разработана для выявления атмосферных взрывов по всему миру. Однако, в изучаемом частотном диапазоне, шумовой фон может влиять на выявления и, в частности, на шум океана, известный как микробаром, как было показано путем описания шумового фона через обработку широкополосной группы на записях МСМ. Действительно, взаимодействия волн океана производят акустический шум почти постоянно, что может скрыть интересные сигналы. Его характеристика важна, и мы используем модели действия волн для моделирования источников микробаром. Видимость такого шума определенной станции должна сильно зависеть от атмосферных условий и возмущений. Для того, чтобы учитывать данный эффект, мы включили спецификации ветра ЕССПП (Европейский центр среднесрочного прогнозирования погоды) в свои модели распространения. Используя продукцию океанических волн двумерного спектра, мы сравниваем амплитуды микробарома и азимуты, подсчитанные из разных моделей распространения с наблюдениями. Данное исследование поможет расширить описание взаимодействия атмосферы и океана, а также разделить эффекты распространения от моделей источников. В свою очередь, улучшенные знания об источниках микробарома позволяют лучше характеризовать события атмосферных взрывов и предоставлять информацию о динамике и возмущениях средней атмосферы, что может быть использовано как ограничения модели.